Three-dimensional Langevin dynamics of N atom scattering from N-covered Ag(1 1 1)

Kang, K.; Shakouri, K.; Kroes, G.J.; Kleyn, A.W.; Meyer, J.

Chemical Physics 560 (2022) 111557

Contents lists available at ScienceDirect

Chemical Physics

journal homepage: www.elsevier.com/locate/chemphys

Three-dimensional Langevin dynamics of N atom scattering from N-covered Ag(1 1 1)

Kai Kang [a,b], Khosrow Shakouri [c], Geert-Jan Kroes [c], Aart W. Kleyn [b], Jörg Meyer [c,*]

[a] Department of Biomedical Engineering, Chengde Medical University, Chengde 067000, China
[b] Institute of Materials, China Academy of Engineering Physics, 610200 Chengdu, Sichuan, People's Republic of China
[c] Leiden Institute of Chemistry, Gorlaeus Laboratories, Leiden University, P.O. Box 9502, 2300 RA Leiden, the Netherlands

ARTICLE INFO

Keywords:
Gas-surface dynamics
Atom scattering
Molecular dynamics
Generalised Langevin oscillator

ABSTRACT

We analyzed the dynamics of N atom scattering from *N*-covered Ag(1 1 1), using the generalized Langevin oscillator (GLO) method and a three-dimensional neural network potential energy surface. Two values for the mass of the surface oscillator were considered in the GLO model to account for the energy exchange with the surface, i.e., that of Ag and that of N. For these mass values different trends were found for the dependence of the ratio of the average final divided by the average initial translational energy on the scattering angle. Using the nitrogen mass gives a trend closer to the experimental results for the dependence of the energy of the in-plane scattered atoms on the scattering angle, but worse agreement with experiment for the angular distribution of the in-plane scattered atoms. Two different algorithms are applied to integrate the stochastic equations of motion in the presence of energy dissipation. Our calculations show that a trivially extended Bulirsch-Stoer algorithm is more efficient than an algorithm based on a Langevin Liouville operator splitting technique, in that it yields the same results with a much larger time step.

1. Introduction

Langevin dynamics can be applied to molecule–metal surface scattering in the case that the coupling of the motion of the incident atom or molecule to that of the surface atoms is mostly mechanical [1]. A three-dimensional (3D) generalized Langevin equation (GLE) model was first proposed to account for the energy exchange between gas particles and surfaces [2,3]. The GLE model divides the surface atoms into two categories: the primary atoms, which interact with the gas particles directly, and the secondary atoms, which designate other surface and bulk atoms.

The model can be further simplified to the generalized Langevin oscillator (GLO) model, where the primary atoms are reduced to a surface oscillator (SO) and the secondary atoms are reduced to a ghost oscillator [4]. In the GLO model the whole potential energy surface (PES) oscillates with the SO and the ghost oscillator is used to describe the energy dissipation into the bulk. This leads to a divide-and-conquer approach in which the Born-Oppenheimer approximation can be used to compute the PES for the incident particle interacting with the ideal surface, to which the SO is coupled by a simple coordinate shift. Despite its simplicity, the GLO model can give quite reasonable results and reveal important details of scattering mechanisms. The GLO method has been applied to e.g. scattering of atoms [5–7] and molecules [4,8–12] from clean metal surfaces, and to atoms scattering from adsorbate covered surfaces [7,13–16], including the simulation of Eley-Rideal (ER) reactions [13–16].

Dohle and Saalfrank have modified the originally SO method by a microscopically motivated coupling term which allows to account for some features of the phononic density of states of the surface [17]. Only very recently a modified GLO model was proposed to allow modeling the change of the barrier height for an activated process with the displacement of the SO, i.e., also considering electronic coupling [18].

Recently, new experiments have addressed the scattering of *N*-atoms from clean [19] and *N*-covered [20] Ag(1 1 1) surfaces. The experiments used translationally broad hyperthermal beams, produced in an arc plasma. These beams contain *N*-atoms in their ground as well as excited electronic states, in addition to N_2 molecules. In-plane scattering was measured. Surprisingly, the experiments showed very similar in-plane angular distributions of the *N*-atoms, and very similar ratios of the average final and translational energies as a function of scattering angle for the scattering from the clean and *N*-covered surfaces [20]. This is not easily understood, as the PESs for the atom interacting with the clean [7] and adsorbate covered [13] surface are rather different. Both the N + Ag

* Corresponding author.
E-mail address: j.meyer@chem.leidenuniv.nl (J. Meyer).

https://doi.org/10.1016/j.chemphys.2022.111557

Available online 27 April 2022

(1 1 1) [5–7,21,22] and the N + N/Ag(1 1 1) [13,14,23] systems have been studied theoretically. Of the theoretical studies on the latter system, one focused on the scattering of the atoms [13], while the two later studies exclusively addressed the formation of N_2 molecules through the ER mechanism [14,23]. All studies were performed utilizing the GLO formalism. The study of the scattering of the atoms can in principle be performed with a 3D PES depending on the three coordinates of the projectile atom [13]; the study of the ER reaction instead requires a 6D PES depending on both the coordinates of the projectile and the target *N*-atoms. In the latter case a surface Ag atom needs to be selected as the SO [14,23], but in the former case one needs to make a choice, as both the mass of the adsorbate N atom and the mass of the surface Ag atom can be selected as the mass related to the SO [13].

In the theoretical study of the scattering of the atoms from *N*-covered Ag(1 1 1), where an N atom is pre-adsorbed on the fcc site of each unit cell, it was stated that GLO calculations were performed using both the mass of Ag and the mass of N as the mass of the SO, but results were only presented using the mass of Ag [13]. This choice was not argued in the paper [13]. Arguments for both choices can be made. The observation that the N + N/Ag(1 1 1) PES shows a far deeper well above the adsorbate *N*-atom, which resides above the fcc Ag(1 1 1) site (-7.493 eV), than above the Ag atom in the hcp site (-2.785 eV), suggests that the interaction will be dominated by the *N*-atom above the fcc-site and that the *N*-atom mass should therefore be used. (On the pristine Ag(1 1 1) surface, the interaction strengths of N with the fcc and hcp sites should be very similar). An argument in favor of using the mass of Ag for the SO is that the dependence of the ratio of the final and initial average translational energy on the scattering angle could be fitted quite well to a binary collision model using the mass of Ag for the target atom. Also, with a probability exceeding 0.35, the ER reaction is quite efficient in the N + N/Ag(1 1 1) system [14,23]. The latter observation suggests that a large percentage of the collisions of the projectile atom with the adsorbate *N*-atom might result in a reactive pick-up event rather than scattering of the projectile atom. It is not clear whether this was known at the time the study of the scattering [13], which appeared earlier than the ER studies [14,23], were performed.

The GLO study using the mass of Ag as that of the SO gave quite reasonable results for the angular distributions of the scattered atoms [13]. A sharp peak found experimentally at the specular angle could not be reproduced. The theorists attributed this discrepancy to the experimental beams containing N atoms in both their ground and excited states [13], following a similar explanation of the presence of a sharp specular peak superimposed on a broad background by experimentalists in experiments on N + Ag(1 1 1) and N + N/Ag(1 1 1) [19,20]. The experimentalists based their explanation [19] on the computed potential energy curves of ground and excited state N atoms interacting with an Ag_{91} cluster, using the embedded cluster and multi-reference single- and double-excitation configuration interaction methods [24]. In one of the states the interaction with the Ag_{91} cluster was much stronger [24], which would be expected to lead to a broad angular distribution [19], while the much weaker interaction in the other state [24] could lead to a strongly peaked distribution near the specular angle. The dependence of the ratio of the final and initial average translational energy on the scattering angle was reproduced quite well, except at grazing scattering angles.

In this paper we re-explore the GLO dynamics of N atoms scattering off the *N*-covered Ag(1 1 1) surface, based on a neural network (NN) PES constructed with more data points than used in the earlier study [13]. We present results using both the mass of N and the mass of Ag as the mass of the SO. The comparison of these results shows that the outcomes of the scattering calculations are quite sensitive to the mass used for the SO. The comparison of our calculations using the mass of Ag with the GLO results of Ref. [13] shows that the calculations are also quite sensitive to the details of the PES used. In addition, we test the efficiency of two algorithms to integrate the stochastic differential equations of motion in the presence of dissipation, i.e., an "in-house modified" Bulirsch-Stoer (BS) algorithm [25] and the so-called "OVRVO flavor" of a recently suggested Langevin Liouville operator splitting technique [26]. As we will show, the "in-house modified" BS algorithm is by far the most efficient one, as it can be used with larger time steps, thereby requiring fewer force evaluations for the same amount of trajectory calculations.

2. Method

2.1. DFT calculation details

Spin-polarized DFT calculations for a 2 × 2 surface unit cell with N atoms adsorbed on each fcc site, a coverage motivated by experiments, are carried out with the VASP code [27–30]. Parameter settings are similar to those in Ref. [13]. However, we found that it is challenging to reach self-consistency. Specifically, magnetization of the system can vary considerably between different electronic ground states of the full system when mapping the PES, which causes energy jumps and thus must be done with proper care. The smearing method used is the Fermi-Dirac method with $\sigma = 0.2$ eV. The DFT energy grid of the total system is calculated for 26 (x,y) positions of the gas N atom, as shown in Fig. 1, where x and y are the Cartesian coordinates denoting the projection of the incident N on the surface. For each (x,y) position, z, the distance of the incident N atom to the surface (which is taken to coincide with the topmost Ag layer) ranges from 6 Å to −1.49 Å in intervals of 0.07 Å. When varying z, the Kohn-Sham wave function and the density from the previous VASP calculation are reused to start the calculation for the next z value. In this way we obtain total energy and magnetization curves that change smoothly with z.

2.2. Construction of the 3D Born-Oppenheimer static surface (BOSS) PES

We use a feed forward neural network (NN) method [31–35] to construct the very corrugated PES of this system. More than 20 different NN topologies have been tried. In all cases, NN training was limited to regions of the PES where the interaction energy was less than 40 eV, which is larger than the energy of interest to the experiments and the molecular dynamics calculations discussed below. Here, the zero of energy is defined as the energy of N atom far from the surface. The best fit we obtained used a NN consisting of 3 hidden layers with 10, 30, and 30 nodes, respectively. The root mean square error (RMSE) in the PES is less than 3 meV in the dynamically important regions. The accuracy of the NN fit is further increased in the most relevant parts of the PES (i.e., the dynamically relevant regions) by assigning higher training weights for energies $\leq$ 20 eV in the same way as done in earlier work [32–34].

2.3. Classical trajectory calculations

Two kinds of dynamics simulations have been carried out based on the 3D NN PES. In one case the static surface approximation is applied, and in the other case the GLO model is applied to include energy exchange and dissipation between the incident gas N atom and the surface. The surface temperature is kept at $T_s = 300$ K, as used in the experiments

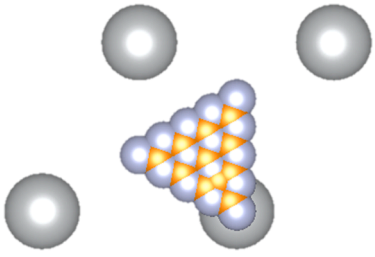

Fig. 1. Configurations of the incident N atom for DFT calculations. Big spheres represent Ag atoms and small spheres represent N atoms. Orange points are additional (x,y) positions other than those in Ref. [13].

[20]. The incident *N*-atoms are started at z = 5.6 Å. In the simulations, the incident polar angle of all incident atoms is kept fixed at $\Theta_i = 60^\circ$ according to the experiments [20], but the azimuthal incidence angle Φ_i is chosen at random, as this incidence angle was not defined in the experiments. However, we have checked that randomly choosing or fixing the incidence azimuth does not affect the dynamics results discussed in this paper. We use a conventional Monte Carlo sampling of the initial position of the incident N atoms projected on the surface, and the initial conditions of the surface and ghost oscillators. As for N scattering from Ag(1 1 1) in Ref. [13], the frequencies associated with the surface and the ghost oscillators are taken as $\hbar\omega_x = \hbar\omega_y = 14$ meV and $\hbar\omega_z = 9$ meV, and the damping matrix diagonal elements are $\hbar\gamma_g = 10$ meV. While this might not seem appropriate for the *N*-precovered surface, we note that other work [8,36] has found qualitative outcomes to be unchanged if the frequencies were changed by two orders of magnitude, and this includes work on the closely related N + N/W(1 0 0) system [36]. We have checked that changing the frequencies likewise has little effect on the outcomes for our system. As we are dealing with a *N*-covered surface and N and Ag atoms have very different masses, we have applied the GLO method by taking both m_{Ag} and m_N as the mass of the SO.

In the experiments [20], the *N*-atom beam has a very broad kinetic energy profile with an average value $\langle E_i \rangle = 4.3$ eV, and a FWHM as large as 5.4 eV, in addition to a high energy tail, which were all reproduced in our simulations. The total number of trajectories N_{tot} was 1.8×10^6 in our simulations using the BS algorithm and 0.9×10^6 using OVRVO, as required to obtain good statistics (see below for these propagation algorithms). The definition of in-plane scattering is the same as in Refs. [13] and [7], i.e. a virtual circular detector with an acceptance angle δ is assumed,

$$\delta = cos^{-1}(sin\Theta_d cos\Phi_d sin\Theta_a cos\Phi_a + sin\Theta_d sin\Phi_d sin\Theta_a sin\Phi_a + cos\Theta_d cos\Theta_a) \quad (1)$$

where the subscripts *d* and *a* refer to the detector and the scattered atom, respectively. The two azimuthal angles are taken with reference to the azimuthal incidence angle and $\Phi_d = 0$ for the in-plane detector. We checked that the number of in-plane scattered atoms is approximately proportional to the value of the acceptance angle δ. Considering that the experimental detector aperture is 1.6°, the number of in-plane scattered atoms is scaled by a factor of 1.6°/δ, which is 0.4 when δ = 4°.

Our criteria at the stop time of a trajectory calculation are: 1) scattered, if the atom reaches the starting value of z with a velocity pointing away from the surface; 2) absorbed, if the atom arrives at z = − 0.5 Å with a negative velocity in z; 3) undetermined, if the atom is not scattered or absorbed at the time the trajectory is stopped.

2.4. Propagation algorithms

Two algorithms, the Bulirsh-Stoer (BS) algorithm and the OVRVO (O = Ornstein − Uehlenbeck, V = deterministic velocity, and R = deterministic position updates) Langevin Liouville operator splitting technique, are used to numerically integrate the classical equations of motion for the static surface approximation and the GLO model. BS is efficient and well established for static surface calculations. In our in-house implementation it has been trivially modified to include the stochastic force terms from the Langevin equation instead of the using the forces resulting from the PES only – analogous to what has been done in previous work with Beeman's algorithm [37].

OVRVO has been constructed specifically for stochastic Langevin equations as employed in the GLO model. It simplifies to the conventional Velocity Verlet algorithm in the static surface case. OVRVO is based on a well-defined error control idea according to the Liouville operator technique [26,38,39]. This technique allows defining a conserved quantity to monitor and thus ensures the accuracy of the numerical integration [40–42]. Even if different implementations of time integration schemes can recover the same continuous (stochastic) differential equations of motion in the limit of an infinitesimally small time step, the dependence on the time step in practical calculations needs to be checked very carefully. In fact, there is still disagreement over the most appropriate integration algorithms and their implementations [43]. Using OVRVO as a reference, we show that our in-house BS implementation yields accurate results for the GLO calculations and is in fact more efficient than OVRVO for this system.

3. Results and discussion

3.1. Convergence of the OVRVO with the BS results

To compare the performance of the OVRVO and BS methods for the GLO simulations, we focus on the GLO calculations using m_{Ag} as the mass of the SO, as also used in Ref. [13]. In Fig. 2 we show the in-plane angular distributions of simulations obtained with this method and SO mass. In the calculations the intensity of the in-plane scattered beam is scaled with respect to the incident beam as $N(\Theta) = N_{ip}/N_{tot}$, where N_{ip} is the number of in-plane scattered trajectories and N_{tot} has been defined above. The intensity we show is the intensity per degree, which is given by $I(\Theta) = N(\Theta)/2\delta$. The statistical error of $I(\Theta)$ is computed as $\sigma = [N(\Theta)(1\text{-}N(\Theta))/N_{tot}]^{1/2}/2\delta$. We can see that the intensity of OVRVO decreases when the time step changes from 10^{-4} ps to 10^{-5} ps, and it gets closer to the result of the BS algorithm, which were obtained with a time step of 10^{-4} ps.

We have checked that the total scattering probability of OVRVO converges to the BS result with decreasing time step, as shown in Table 1. In particular, the scattering probability obtained with the OVRVO method using the smallest time step (10^{-7} ps) is the same as that obtained with the BS algorithm using time steps that are typically three orders of magnitude larger. The same result is obtained if the mass of N is used as the mass of the SO (see Table 2).

The ratio of the average final divided by the initial translational

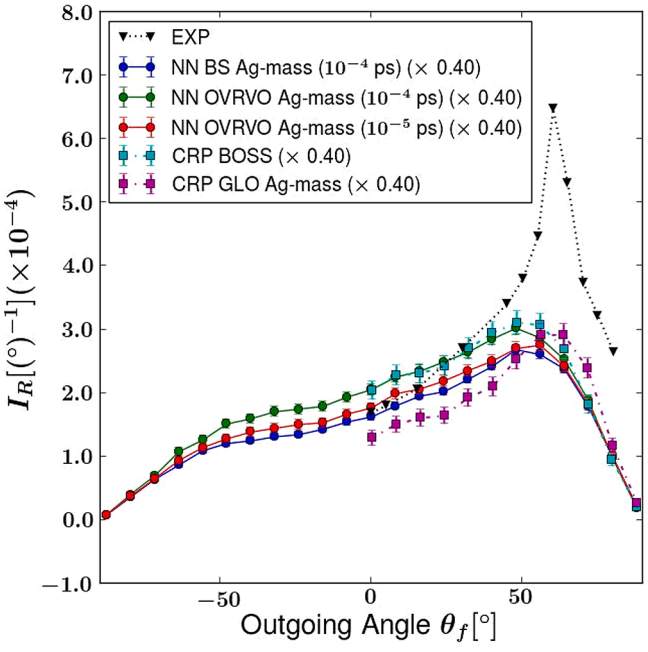

Fig. 2. In-plane angular distribution of scattered N atom. "EXP" is the experimental results of Ueta *et al.* [20]. "NN BS Ag-mass (10^{-4} ps)" means the NN PES and the BS algorithm are used, the SO has the silver mass, and the time step is 10^{-4} ps. "NN OVRVO Ag-mass (10^{-4} ps)" has the same meaning except that the OVRVO algorithm is used, and "NN OVRVO Ag-mass (10^{-5} ps)" has a time step 10^{-5} ps. "CRP BOSS" and "CRP GLO Ag-mass" are BOSS results and GLO results based on a CRP PES respectively, where the silver mass is assigned to the SO in the GLO model [13].

Table 1
Calculated total scattering probability (i.e., the sum of the in-plane and the out-of-plane scattering probability) of incident N atoms in the effusive beam from the OVRVO and BS, with m_{Ag} for the SO. Note that only the initial time step is given for BS.

Time step (ps)	OVRVO				BS
	10^{-4}	10^{-5}	10^{-6}	10^{-7}	10^{-4}
Scattering probability	0.996	0.889	0.840	0.832	0.832

Table 2
Calculated total scattering probability of incident N atoms in the effusive beam from the OVRVO and BS, with m_N for the SO. Note that only the initial time step is given for BS.

Time step (ps)	OVRVO				BS
	10^{-4}	10^{-5}	10^{-6}	10^{-7}	10^{-4}
Scattering probability	0.888	0.495	0.415	0.401	0.401

energy, $<E_f>/<E_i>$, is shown in Fig. 3. The statistical error is computed as $\sigma_E = [\Sigma(R_E\text{-}R_M)^2/N_{bin}(N_{bin}\text{-}1)]^{1/2}$, where the sum is over each bin, $R_E = E_f/<E_i>$, and R_M is the mean ratio of each bin. In assessing the performance of the two propagation methods, we again focus on our own GLO results obtained with the SO mass taken as that of the Ag atom.

The observations made for the change of the OVRVO results for the energy ratio with the change of time step are consistent with those made in Fig. 2 for the angular distribution of the scattered atoms. Specifically, the OVRVO results obtained with the smallest time step are in much better agreement with the BS results.

Fig. 3, Fig. 2, Table 1 and Table 2, imply or show that with decreasing time step the OVRVO results for the energy ratio, the angular distribution of the in-plane scattered atoms, and the total scattering probability will all converge to the BS results for time step of 10^{-4} ps, and that at similar accuracy BS is orders of magnitude more efficient than OVRVO for the present system. To be concise, we will therefore no longer show OVRVO results below. Likewise, except for the case of rebound dynamics the BOSS results obtained with the BS method for our PES are not shown either because they are essentially the same as those obtained in Ref. [13].

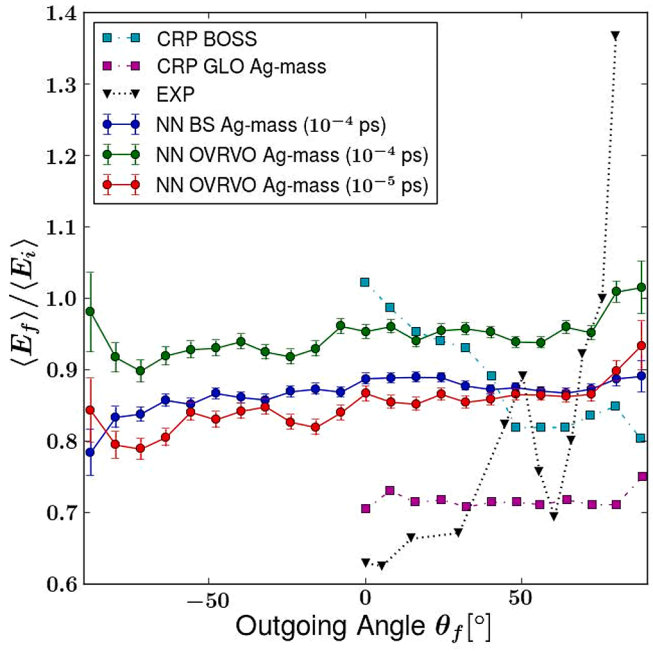

Fig. 3. Ratio of in-plane final-to-initial average energy when the SO has the silver mass. Labels of the curves are the same as in Fig. 2.

3.2. *Langevin dynamics of scattered atoms from an effusive beam*

The in-plane angular distributions and ratio of in-plane final-to-initial average energy are shown in Fig. 4 including the two cases of Ag-mass and *N*-mass SOs, also comparing to experiment. Theoretical calculations based on a ground state PES are in reasonable agreement with the broad part of outgoing angular distribution obtained in experiment if the mass of Ag is used for the SO, or if the surface is treated as static (Fig. 4a). The sharp peak observed in the experimental results near the specular angle is however not observed in the calculations. This peak was attributed by the experimentalists to the excited N atoms in the

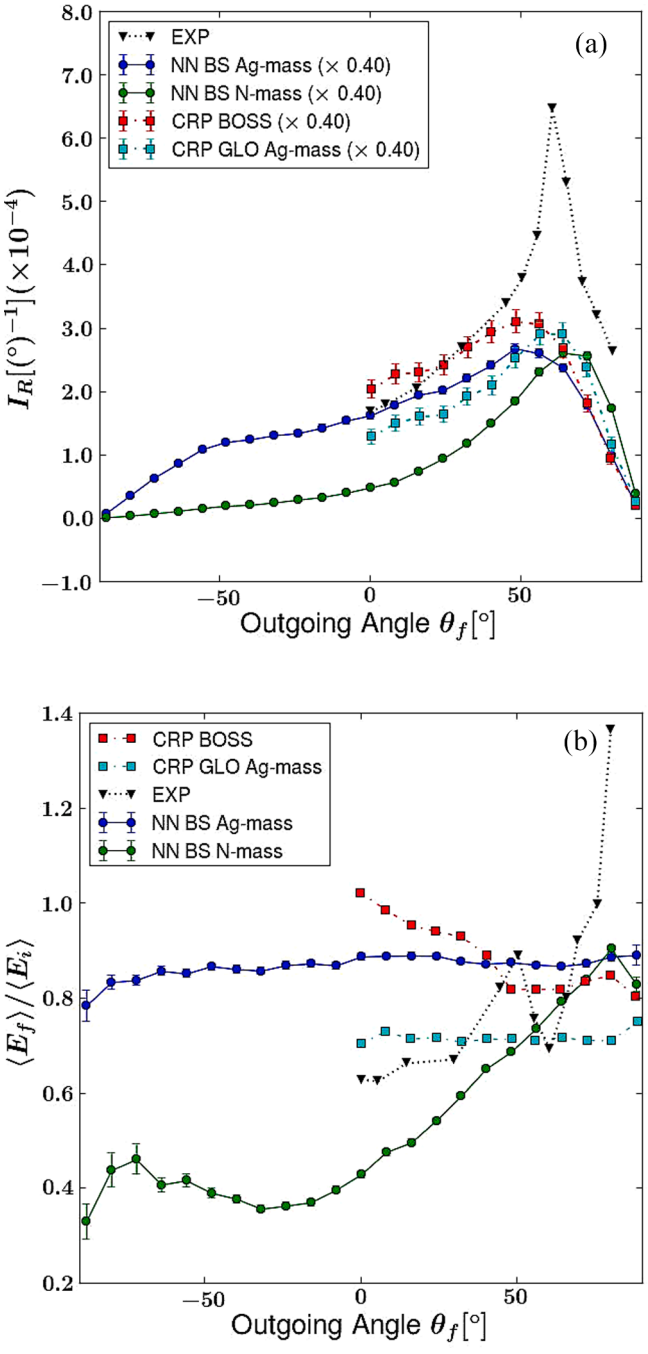

Fig. 4. Results when the SO has the nitrogen or silver mass. (a): In-plane outgoing angular distributions. (b): Ratio of final-to-initial average energy. Labels of the curves are the same as in Fig. 2.

beam for the case of scattering from the *clean* Ag(1 1 1) surface [19]. Interestingly, the specular peak stands out even more in the experiments on N + N/Ag(1 1 1) [20]. The appearance of the peak for the *N*-covered surface, or, more broadly speaking, the fact that the *N*-atom scattering from N/Ag(1 1 1) looks rather similar to that of N scattering from clean Ag(1 1 1), can be explained by the incident *N*-atoms cleaning the *N*-covered surface through efficient Eley-Rideal reaction [14]. This can result in clean Ag(1 1 1) patches. However, this does not yet explain why the specular peak is even stronger in N + N/Ag(1 1 1), suggesting that the *N*-covered surface looks even flatter to electronically excited *N*-atoms than the clean Ag(1 1 1) surface. But in the absence of electronic structure calculations on the interaction of electronically excited *N*-atoms interacting with N/Ag(1 1 1), at this point of time we are not in a position to speculate on the observations noted.

Using m_N as the mass of the SO gives only about half the amount of scattered N atoms as obtained using m_{Ag} as the mass of the SO, which probably reflects more efficient trapping due to more efficient energy transfer in the calculations. Using m_N as the mass of the SO yields much less in-plane scattered *N*-atoms than found experimentally. A possible reason for this is that a substantial part of the collisions with adsorbate *N*-atoms leads to the ER reaction in the experiments, thereby also explaining the high efficiency of this reaction observed in 6D calculations [14,23]. This possibility can be checked by performing 6D GLO calculations treating the motion of both *N*-atoms explicitly. While Juaristi and co-workers published results of 6D calculations for the ER reaction, they did not publish any results of the 6D calculations for the scattering of the *N*-atoms. An alternative explanation holds that our scaling procedure is not appropriate for the comparison with experiment. Fig. 5 shows the comparison with experiment if we do not apply the 0.4 scaling correction to the computed data. In this case the angular scattering data computed with the mass of N for the SO agrees better with experiment than the data obtained with the mass of Ag for the SO. We also note that using m_N or m_{Ag} as the mass of the SO, our outgoing angular distribution is somewhat different from that of Ref. [13]. It is not clear to us why the distributions are not the same if the mass of Ag is used for the SO in both cases (compare the light blue to the dark blue results in Fig. 4a). However, we note that the differences are not large, and that the angular distributions for in-plane scattering may rather sensitively depend on the details of the PESs used.

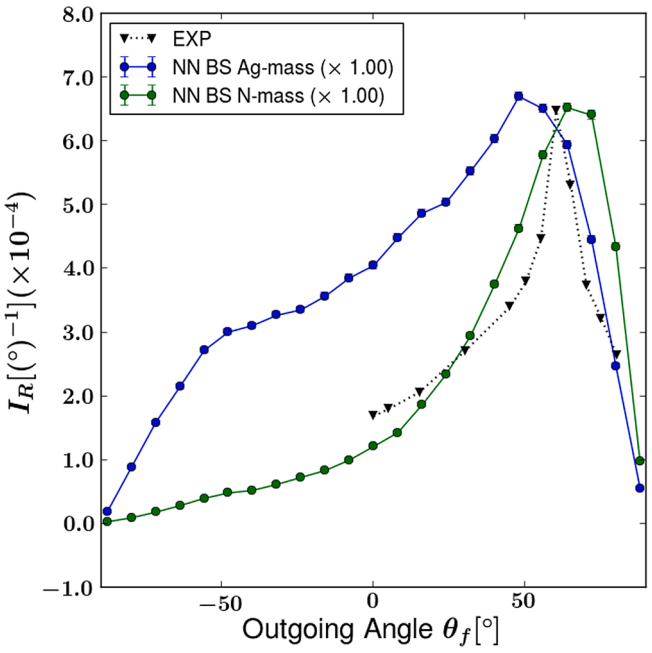

Fig. 5. Unscaled data of in-plane outgoing angular distributions. "EXP" is the experimental results [20].

Our *N*-mass SO curve of the energy ratio reproduces the trend of the experimental result that the final-to-initial average kinetic energy ratio increases with the scattering angle (Fig. 4b), except for the drop near the specular angle and the sharp rise at grazing angles. Our Ag-mass SO curve of the energy ratio does not reproduce the experimental final-to-initial average kinetic energy ratio as a function of scattering angle. This then suggests that the nitrogen mass is the more appropriate choice for the GLO calculations. Again there are discrepancies between our silver mass GLO results and those of Ref. [13]: the latter calculations show much smaller energy ratios than our calculations, which are in good agreement with experiment for small scattering angles. The dependence of the energy ratio on the scattering angle represents an even more detailed result than the in-plane angular scattering distribution, and this ratio would therefore be expected to depend even more sensitively on the PES. We therefore tentatively attribute the differences seen between the GLO Ag mass results in Fig. 4a and Fig. 4b to differences in the details of the CRP and NN PESs used, which could well arise from the use of different DFT calculation settings and fitting methods.

To explain the different trends of the energy ratio, we now plot a somewhat different energy ratio. Specifically, the ratio of the initial average energy of the atoms scattering to the final scattering angle divided by the average translational energy of the incident beam is shown in Fig. 6a as a function of the scattering angle. This is not an experimentally accessible quantity. Likewise, the fraction of the average translational energy of all incident atoms gained by the atoms scattering to a final scattering angle is shown as a function of that angle in Fig. 6b, respectively. For example, if atoms scattering to a specific angle emerge with an energy that is 40% of the average incidence energy of all atoms, this fraction is equal to −0.6. From Fig. 6a we can see that the initial average energies corresponding to each outgoing angle are more like the BOSS curve if the mass of the SO is m_{Ag}, and it is almost flat if the mass of the SO is m_N. This ratio is always larger than 1 for the nitrogen mass, which suggests that in this case the less energetic incident *N*-atoms scatter less in the plane. With increasing scattering angle, the average energy change goes up going from GLO using the silver mass to GLO using the nitrogen mass in Fig. 6b, which means less energy loss to the surface if the mass of the Ag is used for the SO. This results in the two different trends for the two cases. For the silver mass, the initial average energy goes down and the average energy change goes up with scattering angle, which trends cancel each other to give the flat energy ratio seen in Fig. 4b. A similar explanation of this trend, which was based on a somewhat different analysis, was offered in Ref. [13]. For the nitrogen mass, the initial average energy is flat and the average energy change goes up, so the final average energy ratio also goes up as shown in Fig. 4b.

The lack of the drop of the *N*-mass curve in Fig. 4b may be correlated with the absence of the sharp peak seen in the experimental outgoing angular distribution (Fig. 4a). The sharp rise at grazing outgoing angles in the experimental data was attributed to a capture mechanism of low energy N atoms on bare Ag(1 1 1) by Ueta et al. [19]. Calculations based on the CRP PES point out that this phenomenon can be reproduced by the BOSS simulation for the bare Ag(1 1 1) surface, which suggests that this may also be an effect that is not related to any energy dissipation channel [7]. However, on *N*-covered Ag(1 1 1) neither the BOSS nor the GLO calculations yield such a sharp rise. An enhanced reactivity leading to N_2 formation may contribute to this sharp rise. As shown in the simulations with a 6D PES, N atoms with smaller incident energies have higher N_2 recombination efficiency [14], and for a special range of incident azimuthal angle those with larger incident energies have lower N_2 recombination efficiency [23]. Considering the high efficiency of N_2 formation and low sticking probability of high-energy incident N atoms, another possibility is that the sharp rise comes from the clean part of the surface [6,14,44].

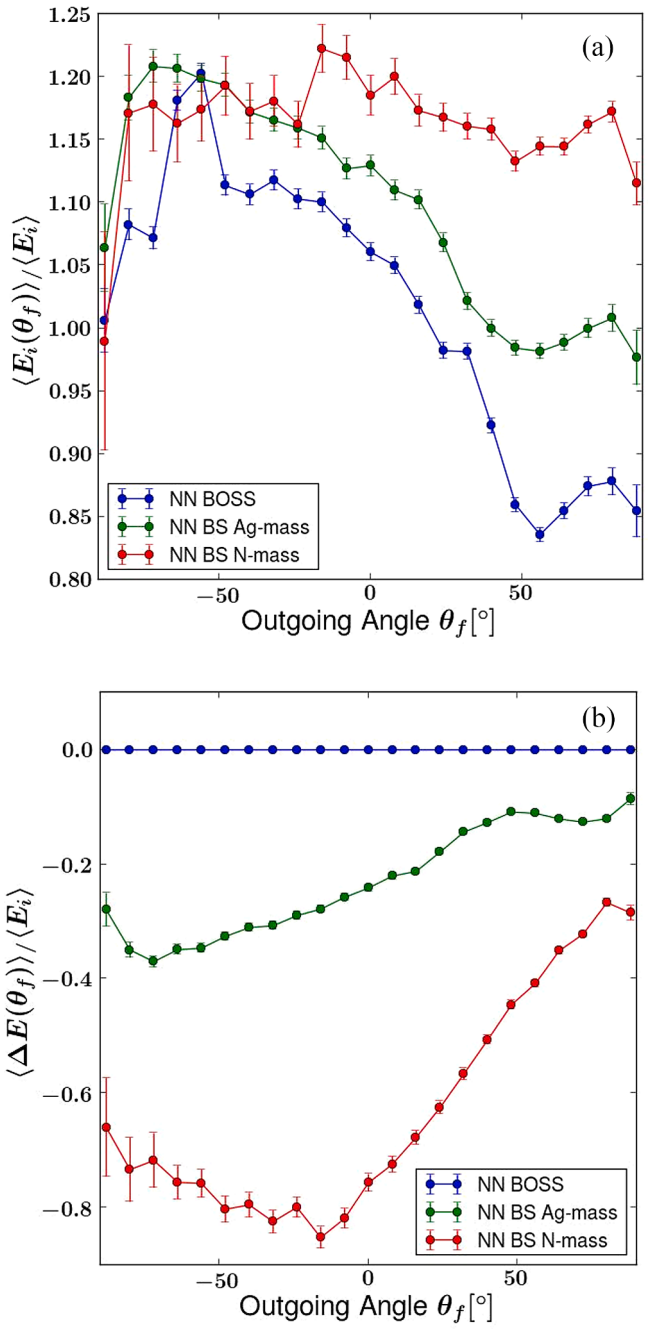

Fig. 6. (a): Ratio of the initial average energy of the atoms scattering in-plane to the indicated angle divided by the average energy of all incident atoms, and (b): fraction of the average incident energy of all atoms gained by the atoms scattering in-plane to the indicated outgoing angle. Labels of the curves are the same as in Fig. 2.

3.3. *Dynamics of scattered atoms from a monoenergetic beam – Number of rebounds*

The presence of high corrugation combined with very deep wells in the PES implies facile interchange between parallel and normal momentum and out-of-plane motion. As a consequence, transient trapping is expected, which can be visualized by considering multiple hops in the scattering, especially at beam energies below the well depth. This is confirmed when plotting the average number of rebounds in the trajectories as a function of outgoing angle for the atoms that scatter in plane. Here the number of rebounds is the number of sign changes in a trajectory of the perpendicular momentum from negative to positive, as in Ref. [13]. The number of rebounds corresponds to the count of this sign change. For monoenergetic beams this number of rebounds changes rapidly with beam energy [13]. Therefore we calculate the average number of rebounds for the same eight incidence energies as used in Ref. [13] (see the insets of Figs. 6 and 10 of this reference) to analyze the rebound dynamics of the in-plane scattered atoms. In each case the total number of trajectories is 10^5.

For the seven higher incident energies, i.e., 1.3, 2.3, 3.3, 4.3, 5.3, 6.3, and 10.0 eV, average numbers of rebounds were obtained that were very similar to those of Ref. [13], and therefore we do not show and discuss these results here. However, a difference appears in the average number of rebounds for the lowest energy of 0.3 eV, as can be seen in Fig. 7. Near the surface normal it is about 20 for the BOSS/NN case, while it is only 7 for the BOSS/CRP case in Ref. [13]. The fact that a substantial difference is only found at the lowest incidence energy, where details of the PESs used should matter most, suggests that also this discrepancy is most likely due to the PESs differing in details as a result of the different DFT calculation settings and fitting methods used. In our GLO calculations, using m_{Ag} as the mass of the SO gave a similar number of rebounds as the BOSS case in the forward scattering region, and an even larger number of rebounds in the backward scattering region. When using m_N as the mass of the SO the number of rebounds of the in-plane scattered atoms decreased dramatically to less than 2. Again, this suggests a more efficient energy transfer, especially for very small incident energies.

4. Conclusions

We constructed a 3D NN PES for N atom scattering from a *N*-covered Ag(1 1 1) surface with more data points than used in Ref. [13]. Classical trajectory calculations using the BOSS and the GLO models were used to analyze the scattering properties. Two algorithms to integrate the equations of motion, i.e. the BS and OVRVO methods, were applied and compared with previous results based on a CRP PES and Beeman's algorithm in Ref. [13]. For the two algorithms used in the present paper we found that OVRVO results converge to the BS results with decreasing time step, and that accurate results can be obtained with the BS algorithm at orders of magnitude smaller computational cost than with OVRVO.

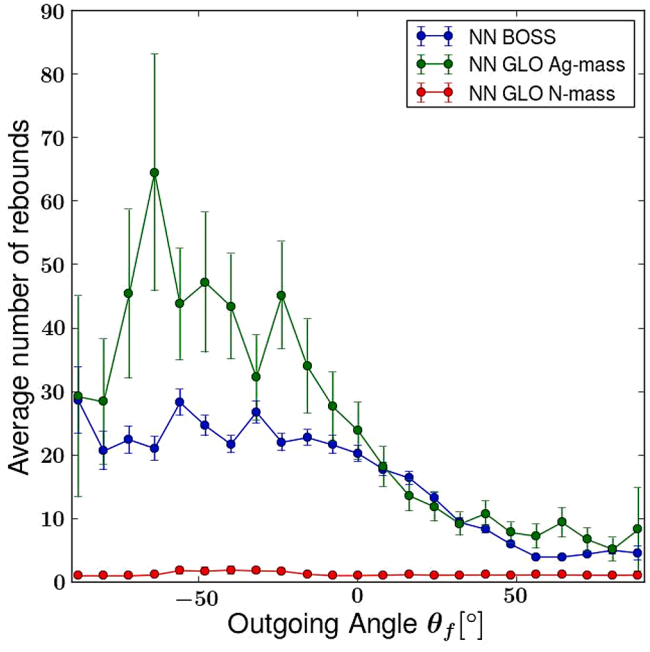

Fig. 7. Average number of rebounds for 0.3 eV monoenergetic beam.

We found that our BOSS results are the same as those obtained in a previous computational study [13], except the average number of rebounds of in-plane scattered atoms of a monoenergetic beam with a very low incident energy (0.3 eV), which number was much larger in our calculations. We attribute this to the sensitivity of the scattering behavior at low incident energy to the details of the PES.

Our GLO results are different from Ref. [13] using either the silver mass or the nitrogen mass as the mass of the SO. For the outgoing angular distribution, the silver mass is large enough to be close to the BOSS result. However, we obtained different ratios of final-to-initial average energy for the two values of the SO mass. The difference arises from the combining effect of initial translational energy and energy loss on the scattering angle. From our results it is not yet clear which mass is best used for the SO in 3D calculations on scattering of N from *N*-covered Ag(1 1 1). Using the nitrogen mass for the SO leads to more efficient energy transfer to the surface and leads to better agreement with the experiments for the energy of the scattered atoms as a function of scattering angle. However, scaled angular distributions of in-plane scattered atoms computed with the Ag mass as the mass of the SO are in better agreement with the experimental results, perhaps because atoms scattering from the adsorbate atoms lead to ER reaction. For more definite conclusions calculations of these two observables will have to be performed that include at least the adsorbed nitrogen atoms explicitly in the dynamics, and compared to the results of the present 3D calculations.

CRediT authorship contribution statement

Kai Kang: Investigation, Formal analysis, Visualization, Writing – original draft. **Khosrow Shakouri:** Software, Methodology, Validation. **Geert-Jan Kroes:** Validation, Resources, Writing – review & editing, Project administration. **Aart W. Kleyn:** Conceptualization, Validation, Writing – review & editing, Project administration. **Jörg Meyer:** Software, Methodology, Resources, Validation, Writing – review & editing.

Declaration of Competing Interest

The authors declare that they have no known competing financial interests or personal relationships that could have appeared to influence the work reported in this paper.

Acknowledgments

This work was supported by the National Natural Science Foundation of China (No. 11547181) for KK, NWO vidi grant 723.014.009 for JM. K. K. thanks Gernot Füchsel and Linsen Zhou for useful discussions.

References

[1] G.-J. Kroes, Computational approaches to dissociative chemisorption on metals: towards chemical accuracy, Phys. Chem. Chem. Phys. 23 (2021) 8962–9048, https://doi.org/10.1039/D1CP00044F.
[2] S.A. Adelman, J.D. Doll, Generalized Langevin equation approach for atom/solid-surface scattering: General formulation for classical scattering off harmonic solids, J. Chem. Phys. 64 (1976) 2375, https://doi.org/10.1063/1.432526.
[3] J.C. Tully, Dynamics of gas-surface interactions: 3D generalized Langevin model applied to fcc and bcc surfaces, J. Chem. Phys. 73 (1980) 1975–1985, https://doi.org/10.1063/1.440287.
[4] J.C. Polanyi, R.J. Wolf, Dynamics of simple gas–surface interaction. II. Rotationally inelastic collisions at rigid and moving surfaces, J. Chem. Phys. 82 (1985) 1555–1566, https://doi.org/10.1063/1.448431.
[5] L. Martin-Gondre, M. Alducin, G.A. Bocan, R. Díez Muiño, J.I. Juaristi, Competition between electron and phonon excitations in the scattering of nitrogen atoms and molecules off tungsten and silver metal surfaces, Phys. Rev. Lett. 108 (2012), 096101, https://doi.org/10.1103/PhysRevLett.108.096101.
[6] L. Martin-Gondre, G.A. Bocan, M. Alducin, J.I. Juaristi, R. Díez Muiño, Energy dissipation channels in the adsorption of N on Ag(111), Comput. Theor. Chem. 990 (2012) 126–131, https://doi.org/10.1016/j.comptc.2012.03.009.
[7] L. Martin-Gondre, G.A. Bocan, M. Blanco-Rey, M. Alducin, J.I. Juaristi, R. Díez Muiño, Scattering of nitrogen atoms off Ag(111) surfaces: a theoretical study, J. Phys. Chem. C. 117 (19) (2013) 9779–9790.
[8] H.F. Busnengo, W. Dong, A. Salin, Trapping, molecular adsorption, and precursors for nonactivated chemisorption, Phys. Rev. Lett. 93 (2004), 236103, https://doi.org/10.1103/PhysRevLett.93.236103.
[9] F. Nattino, O. Galparsoro, F. Costanzo, R. Díez Muiño, M. Alducin, G.-J. Kroes, Modeling surface motion effects in N_2 dissociation on W(110): Ab initio molecular dynamics calculations and generalized Langevin oscillator model, J. Chem. Phys. 144 (2016), 244708, https://doi.org/10.1063/1.4954773.
[10] G.-J. Kroes, J.I. Juaristi, M. Alducin, Vibrational Excitation of H_2 Scattering from Cu(111): Effects of Surface Temperature and of Allowing Energy Exchange with the Surface, J. Phys. Chem. C. 121 (2017) 13617–13633, https://doi.org/10.1021/acs.jpcc.7b01096.
[11] A. Peña-Torres, H.F. Busnengo, J.I. Juaristi, P. Larregaray, C. Crespos, Dynamics of N_2 sticking on W(100): the decisive role of van der Waals interactions, Phys. Chem. Chem. Phys. 20 (2018) 19326–19331, https://doi.org/10.1039/C8CP03515F.
[12] X. Luo, X. Zhou, B. Jiang, Effects of surface motion and electron-hole pair excitations in CO_2 dissociation and scattering on Ni(100), J. Chem. Phys. 148 (2018), 174702, https://doi.org/10.1063/1.5025029.
[13] M. Blanco-Rey, L. Martin-Gondre, R. Díez Muiño, M. Alducin, J.I. Juaristi, Dynamics of nitrogen scattering off N-covered Ag(111), J. Phys. Chem. C. 116 (2012) 21903–21912, https://doi.org/10.1021/jp3074514.
[14] M. Blanco-Rey, E. Díaz, G.A. Bocan, R. Díez Muiño, M. Alducin, J.I. Juaristi, Efficient N2 Formation on Ag(111) by Eley-Rideal Recombination of Hyperthermal Atoms, J. Phys. Chem. Lett. 4 (2013) 3704–3709, https://doi.org/10.1021/jz401850h.
[15] O. Galparsoro, R. Pétuya, J.I. Juaristi, C. Crespos, M. Alducin, P. Larrégaray, Energy dissipation to tungsten surfaces upon Eley-Rideal recombination of N_2 and H_2, J. Phys. Chem. C. 119 (2015) 15434–15442, https://doi.org/10.1021/acs.jpcc.5b04286.
[16] O. Galparsoro, J.I. Juaristi, C. Crespos, M. Alducin, P. Larrégaray, Stereodynamics of diatom formation through Eley-Rideal abstraction, J. Phys. Chem. C. 121 (2017) 19849–19858, https://doi.org/10.1021/acs.jpcc.7b06529.
[17] M. Dohle, P. Saalfrank, Surface oscillator models for dissociative sticking of molecular hydrogen at non-rigid surfaces, Surf. Sci. 373 (1997) 95–108, https://doi.org/10.1016/S0039-6028(96)01143-0.
[18] X. Zhou, B. Jiang, A modified generalized Langevin oscillator model for activated gas-surface reactions, J. Chem. Phys. 150 (2019), 024704, https://doi.org/10.1063/1.5078541.
[19] H. Ueta, M.A. Gleeson, A.W. Kleyn, Scattering of Hyperthermal Nitrogen Atoms from the Ag(111) Surface, J. Phys. Chem. A. 113 (2009) 15092–15099, https://doi.org/10.1021/jp905167p.
[20] H. Ueta, M.A. Gleeson, A.W. Kleyn, The interaction of hyperthermal nitrogen with N-covered Ag(111), J. Chem. Phys. 135 (2011), 074702, https://doi.org/10.1063/1.3615520.
[21] D. Novko, M. Blanco-Rey, M. Alducin, J.I. Juaristi, Surface electron density models for accurate ab initio molecular dynamics with electronic friction, Phys. Rev. B. 93 (2016), 245435, https://doi.org/10.1103/PhysRevB.93.245435.
[22] D. Novko, I. Lončarić, M. Blanco-Rey, J.I. Juaristi, M. Alducin, Energy loss and surface temperature effects in ab initio molecular dynamics simulations: N adsorption on Ag(111) as a case study, Phys. Rev. B. 96 (2017), 085437, https://doi.org/10.1103/PhysRevB.96.085437.
[23] J.I. Juaristi, E. Díaz, G.A. Bocan, R. Díez Muiño, M. Alducin, M. Blanco-Rey, Angular distributions and rovibrational excitation of N2 molecules recombined on N-covered Ag(111) by the Eley-Rideal mechanism, Catal. Today. 244 (2015) 115–121, https://doi.org/10.1016/j.cattod.2014.06.028.
[24] D.B. Kokh, R.J. Buenker, J.L. Whitten, Trends in adsorption of open-shell atoms and small molecular fragments on the Ag(111) surface, Surf. Sci. 600 (2006) 5104–5113, https://doi.org/10.1016/j.susc.2006.08.032.
[25] R. Bulirsch, J. Stoer, Numerical treatment of ordinary differential equations by extrapolation methods, Numer. Math. 8 (1966) 1–13, https://doi.org/10.1007/BF02165234.
[26] D.A. Sivak, J.D. Chodera, G.E. Crooks, Time step rescaling recovers continuous-time dynamical properties for discrete-time Langevin integration of nonequilibrium systems, J. Phys. Chem. B. 118 (2014) 6466–6474, https://doi.org/10.1021/jp411770f.
[27] G. Kresse, J. Hafner, Ab initio molecular dynamics for open-shell transition metals, Phys. Rev. B. 48 (1993) 13115–13118, https://doi.org/10.1103/PhysRevB.48.13115.
[28] G. Kresse, J. Hafner, Norm-conserving and ultrasoft pseudopotentials for first-row and transition elements, J. Phys. Condens. Matter. 6 (1994) 8245–8257, https://doi.org/10.1088/0953-8984/6/40/015.
[29] G. Kresse, J. Furthmüller, Efficiency of ab-initio total energy calculations for metals and semiconductors using a plane-wave basis set, Comput. Mater. Sci. 6 (1996) 15–50, https://doi.org/10.1016/0927-0256(96)00008-0.
[30] G. Kresse, J. Furthmüller, Efficient iterative schemes for ab initio total-energy calculations using a plane-wave basis set, Phys. Rev. B. 54 (1996) 11169–11186, https://doi.org/10.1103/PhysRevB.54.11169.
[31] S. Lorenz, M. Scheffler, A. Gross, Descriptions of surface chemical reactions using a neural network representation of the potential-energy surface, Phys. Rev. B. 73 (2006), 115431, https://doi.org/10.1103/PhysRevB.73.115431.
[32] J. Behler, S. Lorenz, K. Reuter, Representing molecule-surface interactions with symmetry-adapted neural networks, J. Chem. Phys. 127 (2007), 014705, https://doi.org/10.1063/1.2746232.
[33] I. Goikoetxea, J. Beltrán, J. Meyer, J.I. Juaristi, M. Alducin, K. Reuter, Non-adiabatic effects during the dissociative adsorption of O2 at Ag(111)? A first-principles divide and conquer study, New J. Phys. 14 (2012), 013050, https://doi.org/10.1088/1367-2630/14/1/013050.

[34] J. Meyer, Ab initio Modeling of Energy Dissipation during Chemical Reactions at Transition Metal Surfaces, Free University of Berlin, 2012.
[35] I. Goikoetxea, J. Meyer, J.I. Juaristi, M. Alducin, K. Reuter, Role of physisorption states in molecular scattering: a semilocal density-functional theory study on O_2/Ag(111), Phys. Rev. Lett. 112 (2014), 156101, https://doi.org/10.1103/PhysRevLett.112.156101.
[36] E. Quintas-Sánchez, P. Larrégaray, C. Crespos, L. Martin-Gondre, J. Rubayo-Soneira, J.-C. Rayez, Dynamical reaction pathways in Eley-Rideal recombination of nitrogen from W(100), J. Chem. Phys. 137 (2012), 064709, https://doi.org/10.1063/1.4742815.
[37] J.C. Tully, G.H. Gilmer, M. Shugard, Molecular dynamics of surface diffusion. I. The motion of adatoms and clusters, J. Chem. Phys. 71 (1979) 1630–1642, https://doi.org/10.1063/1.438490.
[38] G.J. Martyna, M.E. Tuckerman, D.J. Tobias, M.L. Klein, Explicit reversible integrators for extended systems dynamics, Mol. Phys. 87 (1996) 1117–1157, https://doi.org/10.1080/00268979600100761.
[39] B. Leimkuhler, C. Matthews, Rational construction of stochastic numerical methods for molecular sampling, Appl. Math. Res. EXpress. 2013 (2013) 34–56, https://doi.org/10.1093/amrx/abs010.
[40] G. Bussi, D. Donadio, M. Parrinello, Canonical sampling through velocity rescaling, J. Chem. Phys. 126 (2007), 014101, https://doi.org/10.1063/1.2408420.
[41] R.J. Maurer, B. Jiang, H. Guo, J.C. Tully, Mode specific electronic friction in dissociative chemisorption on metal surfaces: H_2 on Ag(111), Phys. Rev. Lett. 118 (2017), 256001, https://doi.org/10.1103/PhysRevLett.118.256001.
[42] P. Spiering, K. Shakouri, J. Behler, G.-J. Kroes, J. Meyer, Orbital-dependent electronic friction significantly affects the description of reactive scattering of N_2 from Ru(0001), J. Phys. Chem. Lett. 10 (2019) 2957–2962, https://doi.org/10.1021/acs.jpclett.9b00523.
[43] R.W. Pastor, B.R. Brooks, A. Szabo, An analysis of the accuracy of Langevin and molecular dynamics algorithms, Mol. Phys. 65 (1988) 1409–1419, https://doi.org/10.1080/00268978800101881.
[44] K. Kang, A.W. Kleyn, M.A. Gleeson, Kinetic analysis of interaction between N atoms and O-covered Ru(0001), J. Chem. Phys. 143 (2015), 164708, https://doi.org/10.1063/1.4934602.